Mapping topsoil field-saturated hydraulic conductivity from point measurements using different methods

Isabelle Braud[1*], Jean-François Desprats[2], Pierre-Alain Ayral[3], Christophe Bouvier[4], Jean-Pierre Vandervaere[5]

[1] Irstea, UR HHLY (Hydrology Hydraulics), BP 32108, 69616 Villeurbanne Cedex, France.
[2] BRGM D3E NRE, 1039 Rue Pinville, 34000 Montpellier, France.
[3] LGEI – Institut des Sciences des Risques and UMR ESPACE (UMR7300 CNRS, "Antenne Cévenole", Université de Nice-Sophia-Antipolis, Université d'Avignon et des Pays de Vaucluse), Ecole des mines d'Alès, 6 avenue de Clavières, 30319 Alès cedex, France.
[4] Hydrosciences, UMR5569 CNRS, IRD, University of Montpellier, Maison des Sciences de l'Eau, 34095 MONTPELLIER, France.
[5] Institut des Géosciences de l'Environnement (IGE), (CNRS, Grenoble-INP, IRD, University of Grenoble-Alpes), UGA, CS40700, F-38058 Grenoble Cedex 9, France.
[*] Corresponding author. E-mail: isabelle.braud@irstea.fr

Abstract: Topsoil field-saturated hydraulic conductivity, Kf_s, is a parameter that controls the partition of rainfall between infiltration and runoff and is a key parameter in most distributed hydrological models. There is a mismatch between the scale of local in situ Kf_s measurements and the scale at which the parameter is required in models for regional mapping. Therefore methods for extrapolating local Kf_s values to larger mapping units are required. The paper explores the feasibility of mapping Kf_s in the Cévennes-Vivarais region, in south-east France, using more easily available GIS data concerning geology and land cover. Our analysis makes uses of a data set from infiltration measurements performed in the area and its vicinity for more than ten years. The data set is composed of Kf_s derived from infiltration measurements performed using various methods: Guelph permeameters, double ring and single ring infiltrometers and tension infiltrometers. The different methods resulted in a large variation in Kf_s up to several orders of magnitude. A method is proposed to pool the data from the different infiltration methods to create an equivalent set of Kf_s. Statistical tests showed significant differences in Kf_s distributions in function of different geological formations and land cover. Thus the mapping of Kf_s at regional scale was based on geological formations and land cover. This map was compared to a map based on the Rawls and Brakensiek (RB) pedotransfer function (mainly based on texture) and the two maps showed very different patterns. The RB values did not fit observed equivalent Kf_s at the local scale, highlighting that soil texture alone is not a good predictor of Kf_s.

Keywords: Infiltration methods; Topsoil field-saturated hydraulic conductivity; Land cover; Geology; Mapping.

INTRODUCTION

Distributed hydrological models are valuable tools for flood risk management at the catchment or regional scale. Hydrological models generally distinguish two runoff generation mechanisms: i) saturated excess runoff or Dunne runoff (Dunne and Black, 1970), when runoff is generated over saturated areas, and ii) infiltration excess runoff or Horton runoff (Horton, 1933), when rainfall intensity exceeds soil infiltration capacity. Topsoil field-saturated hydraulic conductivity, Kf_s, is a key parameter in controlling infiltration excess runoff. This parameter is generally used in regional scale distributed hydrological models; therefore mapping methods of this parameter are required. The task is difficult because the model mesh scale is much larger (several hundreds m^2 to several km^2) than the scale of available in situ measurements (hundreds of cm^2 to a few m^2) (Davis et al., 1999). Pedotransfer functions, relating soil hydraulic properties to more easily accessible information such as texture, dry bulk density and/or organic matter content, are often used for this purpose. Examples of such pedotransfer functions are those of Clapp and Hornberger (1978), Cosby et al. (1984), Rawls and Brakensiek (1985), the HYPRES functions (Wösten et al., 1999) or ROSETTA (Schaap et al., 2001). Their ability to reproduce observed soil hydraulic properties has been questioned (e.g, Vereecken et al., 2010). Several authors have underlined that those functions, often built using estimations made on undisturbed core samples in the laboratory, may

not be representative of in situ controls of soil hydraulic properties, as they do not sample macropores correctly due to their small sample size (Jarvis et al., 2013). Several papers have highlighted the impact of land cover on topsoil hydraulic conductivity (e.g. Bonell et al., 2010; Gonzalez-Sosa et al., 2010). Recently, Jarvis et al. (2013) presented a global data base of hydraulic conductivity measured in the field using tension infiltrometers. They highlighted that topsoil hydraulic conductivity was only marginally related to soil texture, but that organic carbon content, bulk density and land cover were better explanatory factors of the variability of observed data (see also Jorda et al. (2015) for an update of the study). Our study contributes to this effort of data collection and analysis of controlling factors of Kf_s in the topsoil.

It was conducted in the Cévennes-Vivarais region, a region prone to intense Mediterranean rainfall events that can lead to flash floods especially in the autumn. It was part of the FloodScale project (Braud et al., 2014) aiming at understanding and simulating flash flood generating processes. In this region, several hydrological models were proposed for flash flood simulation and/or forecasting, such as models derived from TOPMODEL (Saulnier and Le Lay, 2009; Vincendon et al., 2016), SCS based models (e.g. Gaume and Bouvier, 2004; Laganier et al., 2014; Naulin et al., 2013), models based on the Richards equation (Vannier et al., 2016) or infiltration excess runoff generation (Ayral et al., 2005), modeling approaches including infiltration excess and sub-surface flow such as the

MARINE model (Garambois et al., 2013; Roux et al., 2011). All of these models require mapping of the variation in saturated hydraulic conductivity at regional scale. A first guess is generally obtained using one of the above mentioned pedotransfer functions, but a hydrological model calibration is in most cases performed starting from this first guess map. This is often achieved using a single multiplicative factor of the map that retains the spatial variability and relative orders of magnitude of the first guess map. For instance, Garambois et al. (2013) have shown that a multiplicative factor ranging from 2 to 20 is needed for saturated hydraulic conductivity in the region to reproduce observed hydrographs which implies that alternative solutions to pedotransfer functions are required in order to provide more realistic maps of saturated hydraulic conductivity that can be used in hydrological models.

In our paper, we take advantage of the large amount of in situ infiltration measurements performed in the study area. However, those infiltration measurements were performed using various techniques such as Guelph permeameters, double or single ring infiltrometers and tension infiltrometers. Several studies have already compared different types of infiltration methods (e.g. Angulo-Jaramillo et al., 2000; Bagarello et al., 2014; Mohanty et al., 1994; Ronayne et al., 2012; Verbist et al., 2013) or some methods for analyzing the data (e.g. Vandervaere et al., 2000; Verbist et al., 2013, Xu et al., 2012). Those studies agree that different methods may lead to differences of several orders of magnitude in the estimated Kf_s, which in turn raises questions about the challenges of pooling our data sets. Thus, the following questions are addressed in the present paper:

1/ Is it possible to pool the data from the infiltration measurements performed with different techniques for the common analysis of Kf_s in the Cévennes-Vivarais region?

2/ Are geology and land cover relevant factors upon which the mapping of Kf_s can be based?

MATERIALS AND METHODS
Description of the available data sets

The data used in this study were collected by different institutes and research teams between 2002 and 2012 in the Cévennes-Vivarais region in south-east of France (Figure 1). The main catchments of the area (black contours in Figure 1) are characterized by steep slopes in their upstream mountainous part (western parts of the catchments), corresponding mainly to granite and schist geology, with a dominant forest land cover. Their downstream parts (eastern part) are flatter, with sedimentary, marl or alluvium geology and are mostly farmed. Another data set is included in this study (blue rectangle in Figure 1). It was collected in the Mercier catchment, a forested and agricultural sub-catchment of the Yzeron periurban catchment, close to the city of Lyon, France in 2008 (Gonzalez-Sosa et al., 2010). The geology is dominated by gneiss and the catchment is prone to Mediterranean influence as is the Cévennes-Vivarais region, with a hydrological response similar to that of the granite forested catchments of the Cévennes-Vivarais. Figure 1 shows a simplified geology map of the Cévennes-Vivarais region and the location of the infiltration measurements used in the present study.

The first two data sets were obtained as part of a study conducted for the Schapi (Service Central d'Hydrométéorologie et d'Appui à la Prévision des Inondations) in order to document Kf_s for use in distributed hydrological models (BRGM data set). BRGM conducted several infiltration measurements campaigns in the Gardons and Avène catchments between 2002 and 2008. Part of the data set is described in Desprats et al. (2010) and in several reports published by Cerdan et al. (2004), Desprats et al. (2005, 2007, 2008), Baran et al. (2006). The infiltration measurements were conducted with two types of devices: Guelph permeameter (GP) (Figure 2a, 143 sampling points) and double ring (DR) infiltrometers (Figure 2b, 164 sampling points). These two data sets will be subsequently referred to as the "GP" and "DR" data sets.

Guelph permeameter principles rely on the measurement of water flux from a cylindrical hole (5 cm in diameter) into a homogeneous, non-saturated porous media. A Mariotte device ensures constant pressure in the cylindrical hole and enables the infiltration rate to be monitored. This device can estimate Kf_s and soil sorptivity (characterizing infiltration capacity as a function of time and initial soil moisture). In our study, Kf_s data were derived from GP measurements at a depth of 15 to 20 cm, using a constant head of 5–10 cm above the hole bottom.
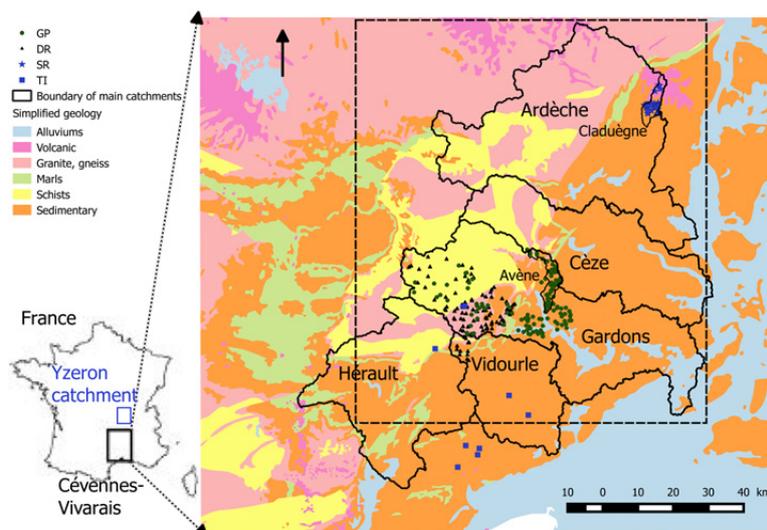
Fig. 1. Location of the study areas in France and simplified geology map of the Cévennes-Vivarais region. The blue rectangle shows the location of the Yzeron catchment in France. The location of the infiltration measurements in the Yzeron catchment (blue rectangle) is not provided here and can be found in Gonzalez-Sosa et al. (2010). The dotted black rectangle corresponds to the location of the land cover map used in the study. The infiltration methods are Guelph Permeameter (GP), Double Ring (DR), Single Ring (SR) and Tension Infiltrometer (TI).
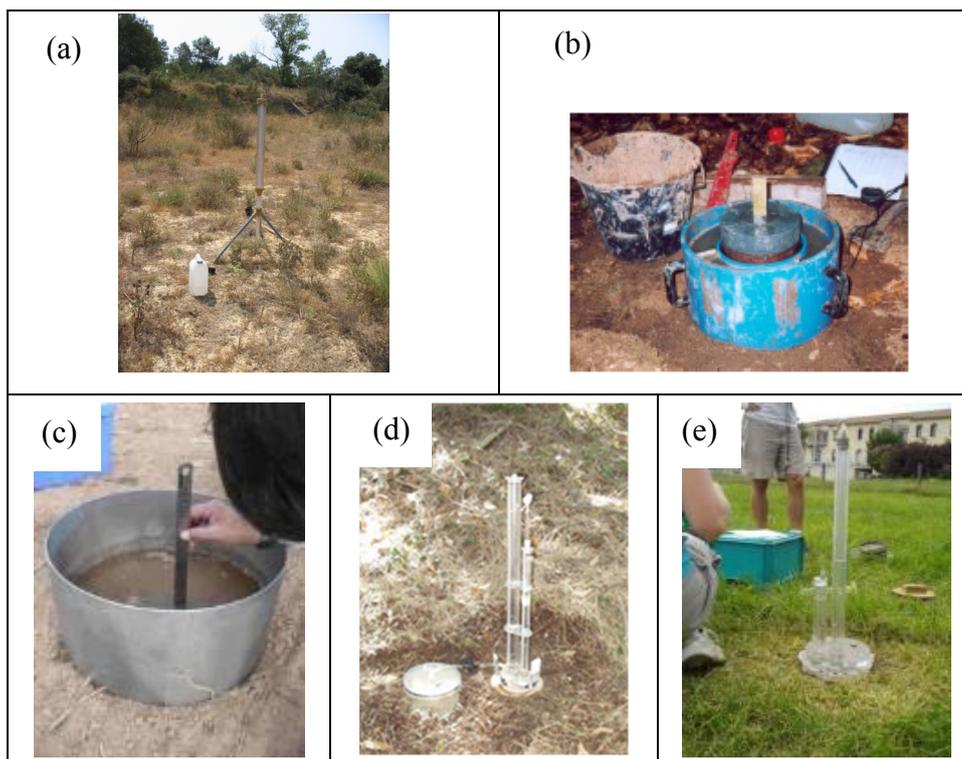
Fig. 2. Photos of the various infiltration methods (a) Guelph permeameter; (b) double ring infiltrometer; (c) Beerkan (single ring) infiltrometer; (d) Tension infiltrometer where the disk has been removed from the tower (SDEC, SW 080 B); (e) Home-made tension infiltrometer from LTHE.

The double ring infiltrometer was composed of two concentric cylinders (40 cm diameter for the inner cylinder) that were inserted into the soil to a depth of 5 cm. The water level was maintained constant in both cylinders and the infiltration rate was measured in the inner cylinder where the lateral diffusion effect was minimized. Kf_s was directly deduced from the surface infiltration volume divided by the cylinder area when a constant flux was reached, assuming that deeper horizons did not perturb the water flux and that the gradient governing water flux was vertical.

For the GP and DR data sets, additional available information was the location, geology and land cover at the sampling locations.

The third data set is the result of single ring (SR) or Beerkan infiltration measurements (Figure 2c) performed in the Mercier sub-catchment of the Yzeron catchment, close to Lyon, France in 2008 (see description in Gonzalez-Sosa et al. (2010)) (57 sampling points) and from a similar data set collected in the Claduègne sub-catchment, in the Ardèche catchment (Figure 1, 50 sampling points) in 2012 (described in Braud and Vandervaere (2015)). The measurements were conducted using a single ring (40 cm inner diameter) positioned at the soil surface after removal of vegetation. Twelve liters of water were introduced into the cylinder without pre-wetting, and the infiltration was measured using a ruler and a chronometer. The infiltration measurements were analyzed following the method proposed in Lassabatère et al. (2006) which exploits the transient infiltration regime and provides retention and hydraulic conductivity curves (see details in Gonzalez-Sosa et al. (2010) and Braud and Vandervaere (2015)). Only Kf_s was considered in this study. This data set will be referred to as the SR data set in the following discussion.

The fourth data set is Kf_s derived from tension infiltration measurements performed in the Cévennes-Vivarais region (Figure 1, 26 sampling points) by the HSM (HydroSciences)

and LTHE (Laboratoire d'Etudes des Transferts en Hydrologie et Environnement) laboratories for this study or other purposes. The tension infiltrometers (TI) used by those laboratories are presented in Figure 2d and 2e respectively, with diameters of 25 and 20 cm. Hydraulic conductivity was derived for the constant flux regime, using the multiple tension method described in Vandervaere (1995) and derived from Ankeny et al. (1991) and Reynold and Elrick (1991). For TI measurements performed with the infiltrometer in Figure 2e, extrapolation of Kf_s from values close to saturation was performed using linear interpolation from a plot of logarithmic hydraulic conductivity as a function of linear tension (five values of applied water potential between –100 and –10 mm). Another method to compute Kf_s was used for the TI measurements performed with the infiltrometer in Figure 2d. As the disk was not directly connected to the water column, the precise adjustment between the disk and water column heights caused some technical difficulties, easily leading to a few mm of uncertainty in the estimation of the applied tension. To overcome the problem, experiments were conducted until a positive soil water head was obtained at the soil surface that could be detected when leakage occurred at the bottom of the disk. The last measured tension was assumed to be –0.1 mm of applied water potential and the hydraulic conductivity estimated at this tension was assumed to be Kf_s. This data set will be referred to as the TI data set.

For the TI and SR data sets, additional information at each sampling site was location, soil texture, organic matter content, dry bulk density, geology and land cover.

In our paper, the following land cover classification is used with the numbers indicated in Tables 1–4: cultivated grassland and crops (10), permanent grassland (11), broadleaf forest (20), coniferous forest (21), lands and moors (22), vineyards and orchards (30). For geology, the classification is: alluviums (100), volcanic rocks (200), granite and gneiss (300), marls (400), schist (500), sedimentary (600).

Table 1. Contingency tables of the original values of log(Kf_s) (mm h^{-1}) by infiltration method and geology/land cover. The chi-squared test has a p-value lower than 0.0001 in both cases. The class numbers for land cover are cultivated grassland and crops (10), permanent grassland (11), broadleaf forest (20), coniferous forest (21), lands and moors (22),vineyards and orchards (30). The infiltration methods are Guelph Permeameter (GP), Double Ring (DR), Single Ring (SR) and Tension Infiltrometer (TI).

Infiltration type	Geology						
	Alluviums	Sedimentary	Granite	Marls	Schist	Volcanic	Total
DR	21	67	29	22	24	0	163
GP	46	28	18	35	16	0	143
SR	0	38	57	0	0	12	107
TI	0	12	6	0	7	1	26
Total	67	145	110	57	47	13	439
	Land cover						
	10	11	20	21	22	30	Total
DR	17	17	70	21	27	11	163
GP	55	21	23	6	5	33	143
SR	34	30	15	7	10	11	107
TI	1	6	7	3	4	5	26
Total	108	74	114	37	46	60	439

Table 2. Mean, standard deviation of log(Kf_s) and number of samples for Guelph Permeameter (GP) and Double Ring (DR) data sets for different combinations of geology and land cover (only combinations common to both infiltration methods are shown, which explains why the total number of points is lower than in Table 1). The class numbers for land cover are cultivated grassland and crops (10), permanent grassland (11), broadleaf forest (20), coniferous forest (21), lands and moors (22),vineyards and orchards (30).

Geology * land cover	DR mean log(Kf_s (mm h^{-1}))	DR standard deviation log(Kf_s (mm h^{-1}))	Number of samles DR	GP mean log(Kf_s (mm h^{-1}))	GP standard deviation log(Kf_s (mm h^{-1}))	Number of samples GP
Alluviums_10	**2.40**	**0.55**	**5**	**1.40**	**0.37**	**20**
Alluviums_11	**2.34**	**0.39**	**8**	**1.36**	**0.34**	**9**
Alluviums_20	3.33	NA	1	1.67	NA	1
Alluviums_30	**1.62**	**0.50**	**5**	**0.84**	**0.56**	**16**
Sedimentary_10	2.15	0.08	2	1.62	0.24	10
Sedimentary_11	**1.97**	**0.30**	**5**	**1.48**	**0.14**	**6**
Sedimentary_20	2.61	0.60	32	1.83	NA	1
Sedimentary_22	2.39	0.67	16	1.99	0.26	2
Sedimentary_30	2.01	0.64	2	1.28	0.31	9
Granite_11	2.77	NA	1	1.40	0.80	2
Granite_20	**2.99**	**0.27**	**20**	**1.83**	**0.31**	**10**
Granite_21	2.58	0.40	5	1.89	NA	1
Granite_22	**2.99**	**0.00**	**3**	**1.57**	**0.40**	**3**
Marls_10	**2.36**	**0.60**	**9**	**1.38**	**0.55**	**22**
Marls_11	2.44	0.88	2	1.57	NA	1
Marls_20	2.12	0.28	2	1.56	NA	1
Marls_21	2.35	0.53	4	1.62	NA	1
Marls_30	**1.77**	**0.33**	**4**	**1.07**	**0.32**	**8**
Schist_10	2.52	NA	1	1.81	NA	1
Schist_20	**2.42**	**0.64**	**15**	**1.70**	**0.34**	**10**
Schist_21	2.26	NA	1	1.59	0.35	4
All	2.50	0.59	143	1.41	0.47	138

Table 3. Mean, standard deviation of log(Kf_s) and number of samples for Single Ring (SR) and Double Ring (DR) + Tension Infiltrometer (TI) data sets (DR+TI) for different combinations of geology and land cover (only common combinations to both infiltration methods are shown). The values used in the regression shown in Figure 7 are highlighted in bold. The class numbers for land cover are cultivated grassland and crops (10), permanent grassland (11), broadleaf forest (20), coniferous forest (21), lands and moors (22),vineyards and orchards (30).

Geology * land cover	DR+TI mean log(Kf_s mm h^{-1})	DR+TI standard deviation log(Kf_s mm h^{-1})	Number of samples DR+TI	SR mean log(Kf_s mm h^{-1})	SR standard deviation log(Kf_s (mm h^{-1}))	Number of samples SR
Volcanic_20	2.26	NA	1	3.25	0.58	6
Granite_10	2.09	0.16	2	2.53	0.58	16
Granite_11	**2.45**	**0.74**	**3**	**2.83**	**0.66**	**24**
Granite_20	**2.88**	**0.32**	**36**	**3.74**	**0.23**	**6**
Granite_21	**2.63**	**0.38**	**6**	**2.89**	**0.24**	**4**
Granite_22	**2.75**	**0.40**	**6**	**3.90**	**0.26**	**4**
Sedimentary_10	**2.59**	**0.45**	**13**	**2.55**	**0.86**	**12**
Sedimentary_11	**2.24**	**0.33**	**12**	**3.06**	**0.43**	**6**
Sedimentary_20	**2.62**	**0.59**	**33**	**3.70**	**0.15**	**3**
Sedimentary_21	**2.75**	**0.62**	**11**	**4.13**	**0.54**	**3**
Sedimentary_22	**2.31**	**0.68**	**22**	**3.39**	**0.38**	**6**
Sedimentary_30	**2.00**	**0.52**	**16**	**2.69**	**0.71**	**8**
All	2.39	0.60	161	2.27	0.59	98

Table 4. Mean, standard deviation of $\log(Kf_s)$ and number of samples for the pooled equivalent data set for different combinations of geology and land cover (only common combinations with more than two samples are shown). The class numbers for land cover are cultivated grassland and crops (10), permanent grassland (11), broadleaf forest (20), coniferous forest (21), lands and moors (22), vineyards and orchards (30).

Geology	Land cover	Class number	Mean $\log(Kf_s$ (mm/hr))	Standard deviation $\log(Kf_s$ (mm/hr))	Number of samples Kfs
alluvium	10	110	2.33	0.49	25
alluvium	11	111	2.29	0.41	17
alluvium	20	120	3.00	0.47	2
alluvium	30	130	1.58	0.67	21
volcanic	10	210	2.08	0.17	6
volcanic	20	220	2.52	0.21	7
granite	10	310	2.30	0.20	18
granite	11	311	2.43	0.30	27
granite	20	320	2.87	0.31	42
granite	21	321	2.56	0.31	10
granite	22	322	2.77	0.31	10
granite	30	330	2.50	0.10	3
marls	10	410	2.31	0.67	31
marls	11	411	2.47	0.63	3
marls	20	420	2.25	0.31	3
marls	21	421	2.40	0.47	5
marls	22	422	1.84	0.38	12
marls	30	430	2.69	0.24	2
schist	10	510	2.35	0.03	6
schist	11	511	2.53	0.58	25
schist	20	520	2.60	0.38	7
schist	21	521	2.51	0.31	6
sedimentary	10	610	2.47	0.41	25
sedimentary	11	611	2.33	0.31	18
sedimentary	20	620	2.63	0.57	36
sedimentary	21	621	2.77	0.55	14
sedimentary	22	622	2.38	0.62	28
sedimentary	30	630	2.12	0.48	24

Building a common pooled Kf_s data set

Figure 3 shows a box plot of Kf_s as a function of the infiltration method. The Kruskal-Wallis test shows that the differences between infiltration methods are significant (p<0.0001). The median DR is about one order of magnitude larger than that of GP, whereas the medians of DR, SR and TI are closer (about a 0.5 order of magnitude difference). Individual values span three to four orders of magnitudes. Several studies have compared different techniques for estimating soil saturated hydraulic conductivity (e.g. Bagarello et al., 2014; Mohanty et al., 1994; Ronayne et al., 2012; Verbist et al., 2013). Mohanty et al. (1994) reported systematically lower values with GP than with TI, but they were dealing with infiltration measurements performed at a depth of 15, 30 or 90 cm and not in the topsoil. Ronayne et al. (2012) found larger values with the DR than with GP in a glacial till soil. In stony soils, Verbist et al. (2013) reported larger values with SR than with DR, the latter being larger than with TI. Bagarello et al. (2014) compared Kf_s values obtained with three methods: 1) infiltration tests where a positive constant head is maintained at the soil surface, 2) infiltration tests using a falling head, and 3) tension infiltrometers. They highlighted the fact that a constant positive head may disturb the soil surface and provoke clogging that may reduce Kf_s values. Differences in Kf_s may also occur because the devices have different infiltration areas and thus cover different soil volumes.

In our case, the SR and DR methods covered the largest radii, whereas the GP and TI methods sampled a smaller area. Regarding the GP method, soil compaction during hole excavation may occur and also clogging due to a constant positive head during the infiltration while soil disturbance can be expected to be virtually absent with TI methods. However, for the latter, an underestimation of Kf_s cannot be excluded since the

extrapolation to zero soil water pressure may neglect the potential influence of the macropores network. All those differences in measurement protocols require caution when analyzing the pooled data.

Pooling was conducted in two steps. In Figure 3, GP and DR data sets were significantly different (p<0.0001) and we chose to pool these two data sets first, trying to establish a relationship between them. We first worked with the GP and DR data sets because the sampling points from these methods spanned the largest combinations of geology and land cover (Table 1). In addition, such pooling had already been performed successfully by Desprats et al. (2010) for these two methods. They computed average values for different combinations of geology and land cover and fitted the following relationship using the averages per geology * land cover:

$$Kf_{s\_DR} = 47.422 \exp\left(0.0502 \, Kf_{s\_GP}\right) \qquad R^2 = 0.80 \qquad (1)$$

In our study additional sample points were available so we updated this relationship. In addition, as the distribution of Kf_s was found to be log-normal, we chose to compute the relationship on $\log_{10}(Kf_s)$, expressed as $\log(Kf_s)$ in the following discussion, instead of using the exponential relationship of Desprats et al. (2010). The advantage of our solution is that it fits a linear relationship rather than a non-linear one which allows uncertainty on the regression coefficients to be easily computed. Working with $\log(Kf_s)$ also allowed us to reduce the differences in orders of magnitude among the data sets. Furthermore, the tests described in the Results section were performed to choose the method (DR or GP) used to compute the "equivalent" Kf_s used in the subsequent analysis. The DR method was chosen after those tests which allowed us to reduce the data sets to three infiltration methods.
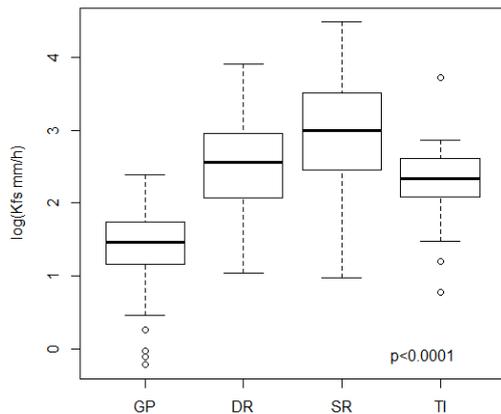
Fig. 3. Box plot of the original data set of field-saturated hydraulic conductivity Kf_s (mm h^{-1}) (log scale) for the different infiltration methods. In the box plots, the box boundaries indicate the 25th and 75th percentiles, the bold line indicates the median, and the top and bottom whiskers indicate the 10th and 90th percentiles. The open circles are the outliers.

In the second step, Kruskal-Wallis tests were conducted to determine wheather or not the three remaining types of infiltration methods were significantly different. The DR and TI values were not significantly different whereas the SR values were significantly different from DR and TI. Therefore we tried to establish a relationship between the SR and DR + TI data sets which would enable all the data to be pooled together for subsequent analysis. This analysis consisted mainly in comparing various distributions, according to geology and land cover information, as they were the only available common factors for all the sampling points.

The Kruskal-Wallis test was used to compare the distributions and statistical analyses were performed using R software (R Core Team, 2014).

Mapping Kf_s

A mapping procedure was proposed based on the statistical analyses for pooling the data presented in the previous section. It relies on geology and land cover information (see details in the Results section and in Table 4). A 30 m resolution land cover map, produced by Andrieu (2015), was available for part of the study area (see black rectangle with broken line in Figure 1). It was derived from multiple Landsat images made in 2013 using an unsupervised classification method (Andrieu, 2015) with the following nomenclature: 1= uncovered soils, urban, roads, rocks; 2= early crops (spring vegetation growth); 3= late crops (summer vegetation growth); 4= vineyards, bare soils, rocks; 5= grasslands; 6= broadleaf forests; 7= mixed forests; 8= coniferous forests; 9= shrublands; 10= water bodies. The map was reclassified to match the land cover classification used in our study by merging classes 2 and 3 to match our class 10 (cultivated grassland and crops); class 5 was assumed to be permanent grassland (class 11); class 7 was merged with class 6 to match our class 20 (broadleaf forest) and class 9 was assumed to be our class 22 (lands/moors).

A vector geology map from BRGM was available at the 1/1000000 scale and the geology layer was simplified according to the classes listed above (see Figure 1). This map was converted to raster layer at the land cover map resolution and reclassified according to the combinations proposed in Table 4 and the average log(Kf_s) of each combination was assigned to the class for mapping.

This map was compared to the results obtained by Manus et al. (2009) and Vannier et al. (2016) using the Rawls and Brakensiek (1985) pedotransfer functions (RB85) over the area. For this mapping, these authors used a soil data base from the IGCS (Inventaire Gestion et Conservation des Sols, https://www.gissol.fr/tag/igcs) program, associated with a vector map of soil cartographic units at the 1/250000 scale (pedology map in the following discussion). It was possible to derive maps of clay, sand and silt contents, and porosity from this information (Manus et al., 2009), which were used to compute Kf_s from the RB85 formula (see details in Manus et al. (2009) for the Languedoc-Roussillon region and Bonnet (2012) for the extension to the whole Cévennes-Vivarais region). The values obtained at the infiltration measurement locations were extracted and compared to the values derived from Table 4, to assess the predictive power of the RB85 pedotransfer function.

RESULTS
General description of the data sets

Table 1 shows the contingency tables of number of sampling for the various infiltration tests (original data set) by infiltration method and geology and land cover. In both cases, the chi–squared test had a p-value <0.0001, showing that the points distribution was far from being homogeneous, in particular in terms of geology. Indeed, two geologies: alluviums and marls were only sampled using DR and GP methods, whereas volcanic rocks were only sampled using the SR and TI methods. Nevertheless, most of the samples were taken for the dominant geology classes in the area: sedimentary, granite and schist. The sampling is somehow more homogeneous for land cover, but TI data are much less abundant, given the longer time required to perform this kind of infiltration tests. Three points with very low Kf_s values were removed from the GP data set for subsequent analysis as they were outliers.

For the SR and TI data sets, soil texture was available, so it is possible to show the sampling points in the USDA textural triangle (Figure 4). We can see that the data span over a large range of clay and sand contents. Nevertheless, coarse soils (sand and loamy sands) are hardly represented.
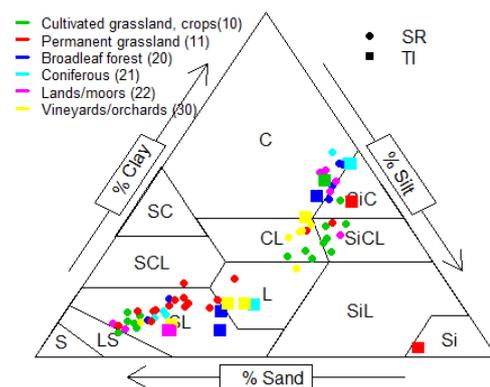
Fig. 4. Location of the Single Ring (SR) and Tension Infiltrometer (TI) data sets in the USDA textural triangle. The numbers in parenthesis are the land cover class numbers.

Results obtained when pooling all data sets

Table 2 presents the average and standard deviation of the GP and DR data sets for different combinations of geology and land cover information. Only the combinations with more than two samples (bold figures in Table 2) were retained to build the

relationship between the values of $\log(Kf_s)$ in the two data sets. Two regressions were tested (Figure 5): one with equal weights for all the points, one with non-equal weights (see documentation of the *lm* function in R software: http://127.0.0.1:28603/library/stats/html/lm.html), w_i, inversely proportional to the average variance of $\log(Kf_s)$ at each point computed as: $w_i = 1/((var(\log(Kf_{s\_DRi})) + var(\log(Kf_{s\_GPi})))/2)$ where $_i$ refers to one combination of geology and land cover. The equal-weight regression was chosen as it resulted in a higher determination coefficient ($R^2 = 0.665$, $p = 0.0045$) than when non-equal weights were used ($R^2 = 0.566$, $p = 0.012$). The corresponding equation was the following:

$$\log\left(Kf_{s\_DR}\right) = \left(1.3148 \pm 0.32\right) * \log\left(Kf_{s\_GP}\right) \\ + \left(0.4712 \pm 0.46\right) \quad R^2 = 0.66 \quad p = 0.0045 \tag{2}$$

Although each point had a large standard deviation, the relationship was quite good, with an R^2 value of 0.665. This determination coefficient is lower than that of Eq. (1) by Desprats et al. (2010), but Eq. (2) was not established with exactly the same data set. In addition, fitting a linear regression allows providing easily uncertainty bounds for the regression coefficients. Eq. (2) shows that the uncertainty on the intercept is higher than that of the regression slope. More importantly, Eq. (2) is more consistent with physical principles than Eq. (1), previously established by Desprats et al. (2010) on Kf_s values instead of $\log(Kf_s)$. Indeed, in Eq. (1), Kf_{s_DR} tends towards a constant value when Kf_{s_GP} tends towards zero, which was not very satisfactory. This problem is avoided with Eq. (2).

Once this equation was established, for each sample point where a GP value was measured, an equivalent DR Kf_{s_DR} value was computed using Eq. (2). Similarly for each sample point at which a DR value was measured, an equivalent GP Kf_{s_GP} value was computed using the regression between GP and DR values. These values were used to draw box plots of $\log(Kf_s)$ for three infiltration methods (GP, SR and TI) and (DR, SR and TI) (Figure 6a and Figure 6b, respectively). The Kruskal-Wallis test showed that GP and SR, and GP and TI data were all significantly different ($p < 0.0001$) and could not be analyzed together.

On the other hand, DR and TI data did not have significantly different distributions ($p = 0.25$) and could be analyzed together. The SR data were still significantly different from the other two data sets ($p<0.0001$). Therefore, similarly to what was done for the DR and GP data sets, we tried to establish a relationship between the SR and DR+TI data sets. For both data sets, geology and land cover information was used to compute averages for each geology * land cover class, as the Kruskal-Wallis test showed that the $\log(Kf_s)$ values were significantly different for geology and land cover classes with p values < 0.0001. Table 3 shows the averages and standard deviations for both types of infiltration methods and Figure 7 shows the relationships that were fitted using either equal weights (black line, $R^2=0.25$, $p = 0.07$) or with weights inversely proportional to the variance of each point (blue line, $R^2 = 0.32$, $p = 0.05$). This second equation, with the highest determination coefficient and the lowest p value, was retained for further analysis and reads:

$$\log\left(Kf_{s_{DR+TI}}\right) = \left(0.33 \pm 0.14\right) * \log\left(Kf_{s\_SR}\right) \\ + \left(1.49 \pm 0.50\right) \quad R^2 = 0.32 \quad p = 0.05 \tag{3}$$

The determination coefficient is much lower than in Eq. (2) but still significant at the 5% level. Table 3 shows that only two geologies could be used to establish this relationship: granite and sedimentary. We must therefore assume that the relationship is also valid for all the other combinations of geology and land cover information, which is a limitation of the results as all available combinations were not used in establishing the relationship.

The Kf_s values of the SR data sets were converted to an equivalent DR+TI value using Eq. (3). This pooled equivalent set of values is the one used subsequently for mapping $\log(Kf_s)$. Once again, the Kruskal-Wallis test showed that geology and land cover were discriminating factors in the distribution of $\log(Kf_s)$ and averages and standard deviations were computed for the different combinations of geology and land cover information (Table 4 and Figure 8). In the next section the average values per geology and land cover classes are proposed for mapping $\log(Kf_s)$ at the regional scale.
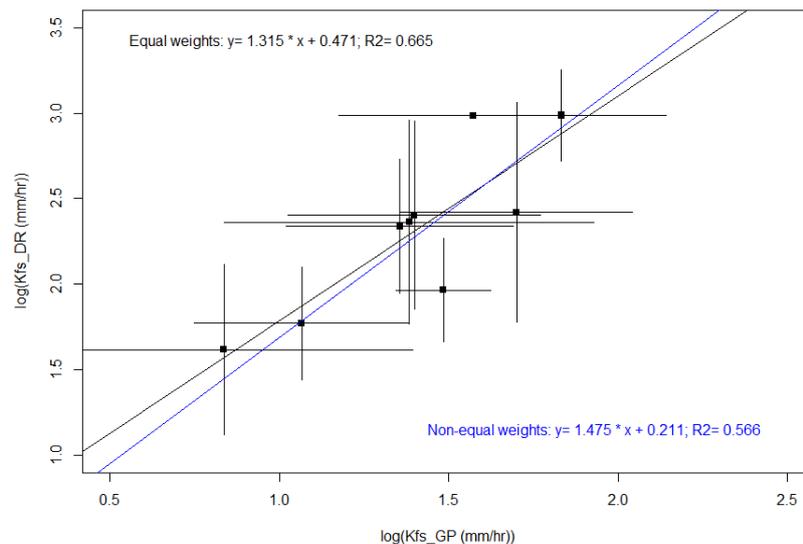
Fig. 5. Regression between $\log(Kf_s)$ (mm h^{-1}) for Guelph permeameter (GP) and Double Ring (DR) infiltration methods. The points are mean values per geology * land cover classes and the vertical and horizontal lines correspond to one standard deviation. Two regressions are shown: the first one with equal weights for all points (black), the second with weights inversely proportional to the variance of each point (blue).
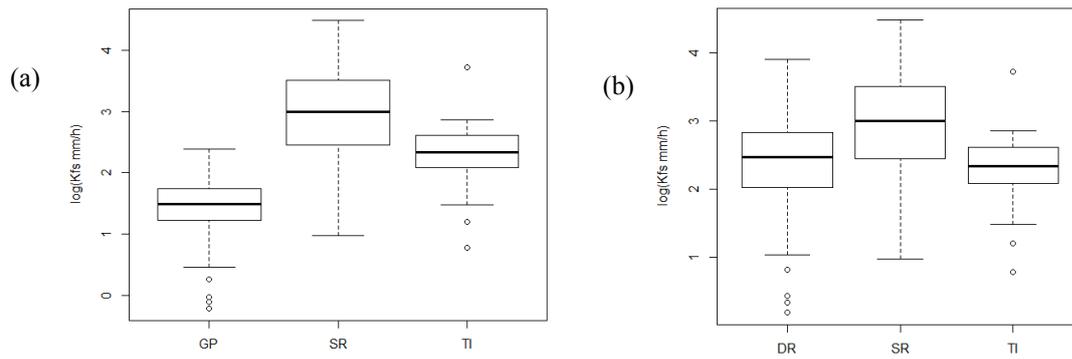
Fig. 6. Box plots of all log(Kf_s) values when (a) DR values of the BRGM data set are converted to GP values using Eq. (2) and (b) GP values of the BRGM data are converted to DR values using the regression between GP and DR values.
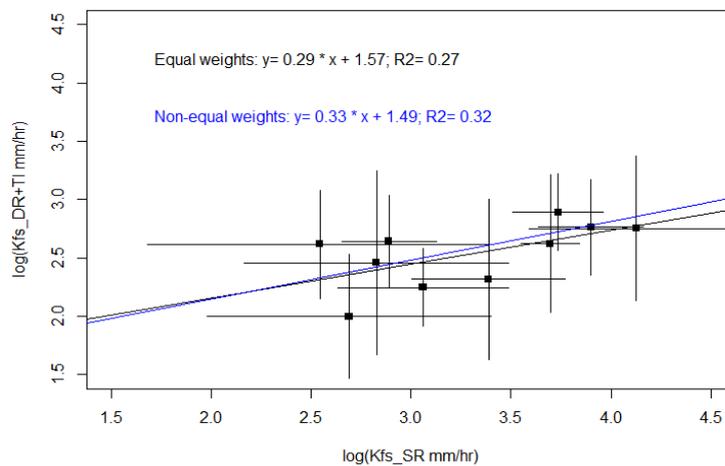
Fig. 7. Regression between log(Kf_s) (mm h^{-1}) for Single Ring (SR) and Double Ring + Tension disk Infiltrometer (DR+TI) infiltration methods. The points are mean values per geology * land cover classes and the vertical and horizontal lines correspond to one standard deviation. Two regressions are shown: the first one with equal weights for all points (black), the second with weights inversely proportional to the variance of each point (blue).
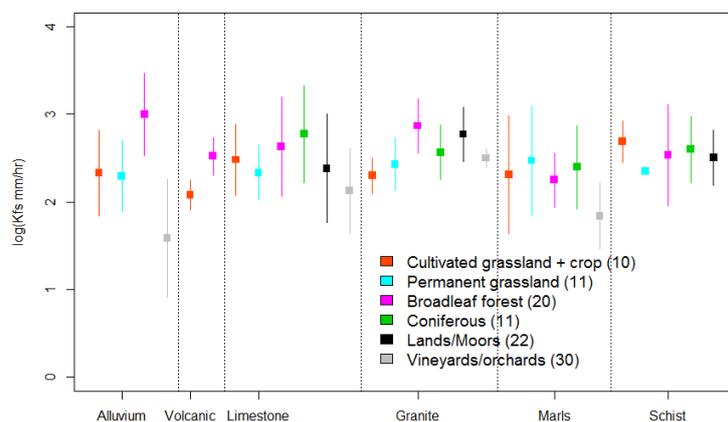
Fig. 8. Bar plot of average log(Kf_s) (mm h^{-1}) plus one standard deviation for the different combinations of geology and land cover derived from the final homogenized data set.

Mapping topsoil field-saturated hydraulic conductivity

The average log(Kf_s) values provided in Table 4 for each combination of geology (Fig. 1) and land cover allowed the log(Kf_s) to be mapped for the three main catchments in the area (Ardèche, Céze and Gardons, see rectangle in Figure 1). In the resulting map, no value was assigned to pixels that had a geology and land cover combination not present in Table 4 (mainly land cover 1 (rocks and urban areas), but also some land cover

for volcanic rocks). The results are shown in Figure 9a and the corresponding map obtained using the RB85 pedotransfer function is shown in Figure 9b. Note that there are differences in orders of magnitude between the two maps, which is expressed as lighter blue colors for the RB85 map. The log(Kf_s) range of the RB85 map is −1.08 to 1.97 corresponding to a Kf_s range of 0.083 to 95.5 mm h^{-1}, whereas the map derived from geology and land cover (Table 4) leads to a range of 1.58 to 3.00, corresponding to Kf_s values ranging from 38.0 to 996.6 mm h^{-1}.
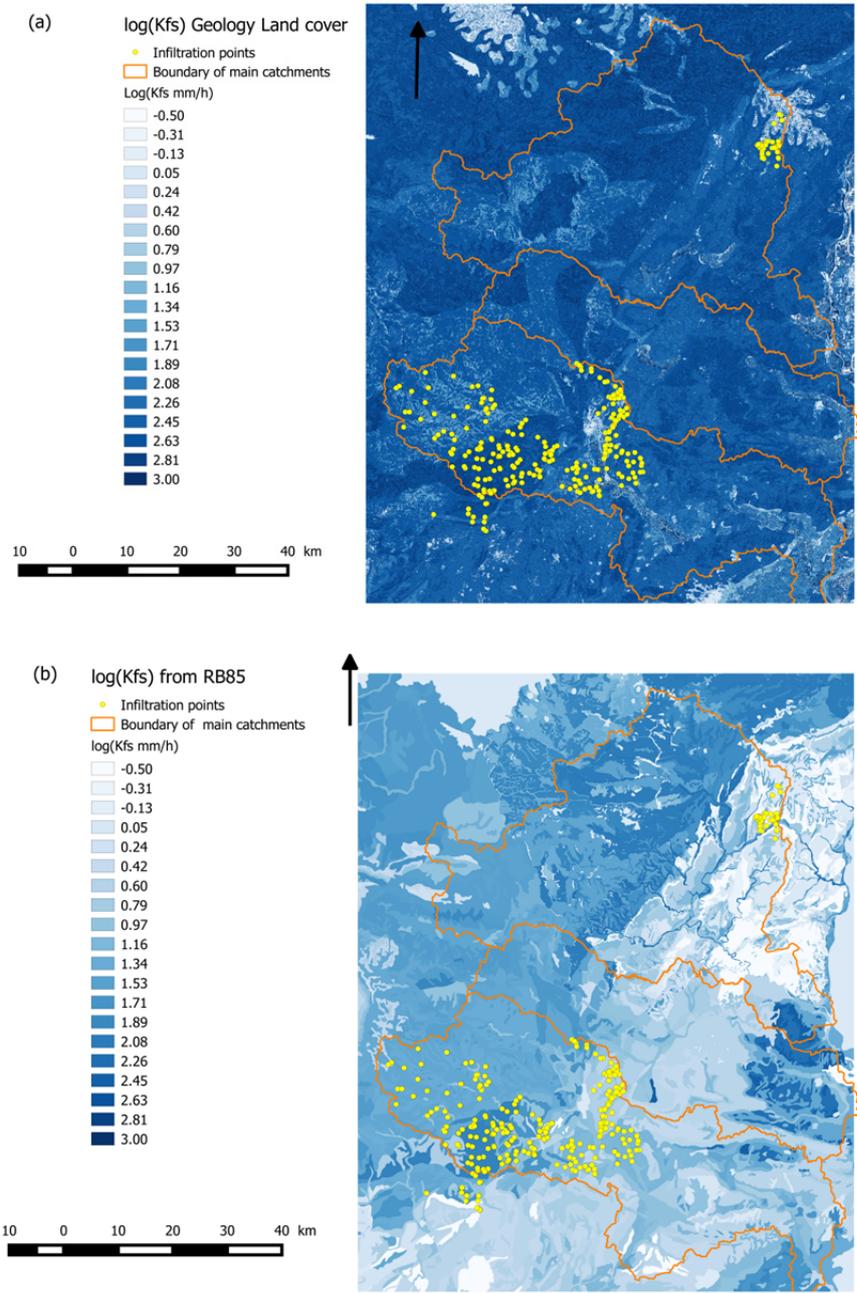
Fig. 9. Maps of log(Kf_s) for part of the Cévennes-Vivarais region using (a) the geology and land cover maps and the results of Table 4 and; (b) the pedology map and Rawls and Brackensieck pedotransfer function RB85.

If other pedotransfer function models such as those using only textural information (e.g; Cosby et al., 1984) had been used, a smaller range would have been obtained as Manus et al. (2009) showed that RB85 was the pedotransfer function leading to the largest range of Kf_s as compared to the other methods they tested in this area. The patterns of Kf_s are also different in the two maps. Figure 9b reflects the pedology map and soil cartographic units, whereas Figure 9a is mainly shaped by the geology map, modulated by the land cover map, which has a much higher resolution. Figure 10 shows the comparison of the values of the two maps at the infiltration tests sampling locations. It demonstrates that RB85 log(Kf_s) values are much lower than the values obtained in the present study. The data points are not correlated at all, showing that pedotransfer functions not taking into account land cover information is not a good predictor of the spatial variability of Kf_s in the area.

DISCUSSION

In this paper, we propose a simple method, based on statistical tests analyzing differences in distributions and simple regressions to pool together values of topsoil field-saturated hydraulic conductivity, Kf_s, obtained using different infiltration methods, mainly tension infiltrometers (TI) and methods based on positive heads (Guelph permeameter (GP), double ring (DR) infiltrometer, single ring – Beerkan (SR) infiltrometer). Our results are consistent with previous studies that indicate that different methods may lead to differences of several orders of magnitude in the estimated Kf_s. Thus, much lower values were obtained with GP than with the other methods which could be expected as the GP measurements were performed between 15 and 20 cm depth, whereas the depth was of less than 10 cm for the other methods. We might expect larger Kf_s values with

positive head infiltration methods than with TI, since the extrapolation procedure for the latter may give underestimated values. However, Bagarello et al. (2014) have reported, for some sampling points, lower Kf_s values when a positive head is maintained during the measurements than when a falling head or even tension infiltrometers are used. With a positive pressure head, soil particles may be disturbed and clog the soil surface and top soil. For the SR data set, we only experienced clogging at a few sampling points. In addition, the infiltration measurements were mainly performed on vegetated surfaces and although vegetation was cut before the infiltration test, the root network was still present, which should limit the clogging problem. The sampling surface is also generally lower with TI than with the other methods. In our data set, TI leads to values of the same order of magnitude as the DR method. Nevertheless, the number of sampling points with TI was much lower (Table 1) than with the three other methods. This could reduce the impact of TI data on the final results.

The standard deviations of the regression coefficients in Eq. (2) and Eq. (3) are quite large, showing that the fitted regressions have a large uncertainty that is propagated to the final map of Fig.9a. In addition, only two geologies could be used in establishing Eq. (3): granite and sedimentary. We had to assume that the relationship was also valid for all the other combinations of geology and land covers, which was a limitation of the study. All those uncertainties should be kept in mind when considering using the final map in hydrological models for instance.

It was not possible to include soil texture, organic carbon and dry bulk density in our analysis because they were only available for the SR and TI data sets. It would have been interesting to perform the kind of analyses proposed by Jarvis et al. (2013) and Jorda et al. (2015) on those data, but the sample size was too small. Nevertheless, similarly to these studies, our analysis points out the main impact of land cover on Kf_s, calling for an inclusion of land cover in soil surface Kf_s mapping methods. In addition, near saturated hydraulic conductivity at -20 mm applied water potential (K(–20 mm)) was also acquired using mini-disk infiltrometers (Decagon Devices Inc., Pullman, WA, diameters 4.5 and 8 cm) at the locations of the SR data sets (Gonzalez-Sosa et al., 2010; Braud and Vandervaere, 2015). The results showed the Kf_s /K(–20 mm) ratio ranging between 21 and 570, which highlights the influence of macropores close to saturation. This change in hydraulic conductivity is generally not taken into account in hydrological models, but it would be preferable to do so. The adaptation of classical hydraulic conductivity functions such as those proposed by Jarvis (2008) or Gonzalez-Sosa et al. (2010) could be used. On the other hand, for deeper horizons (< 10–30 cm) where land cover is supposed to be less influential (Jarvis et al., 2013), a map such as the one proposed in Figure 9b, computed using pedotransfer functions for the deeper horizons could be relevant. Infiltration data of deeper horizons are much less abundant as most methods require pedological pits to be dug, and using pedotransfer functions is thus the easiest available method. In this context, the GP method is practical since measurements can easily be made at deeper horizons in replicated auger made by drilling.

The mapping method proposed in the present paper is quite simple and only relies on two easily accessible maps: geology and land cover. Ferrer et al. (2004) proposed a map of soil saturated hydraulic conductivity for Spain, based on interpolation of point data. They showed that the final map was consistent with the geology map, indirectly pointing out the relevance of this factor for Kf_s mapping. In the Mercier catch-
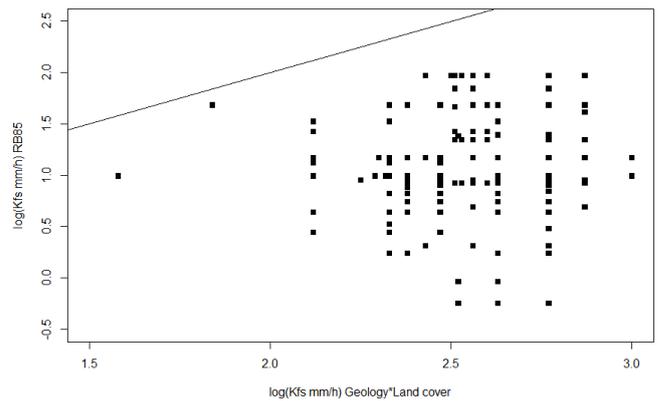
Fig. 10. Comparison of log(Kf_s) obtained at the infiltration sampling points from the map obtained using the RB85 pedotransfer function (Figure 9b) and the geology and land cover map based on Table 4 (Figure 9a).

ment (6.7 km^2), where geology was homogeneous (gneiss), Gonzalez-Sosa et al. (2010) proposed land use as a main factor for mapping Kf_s, based on a high resolution field scale land cover map. The advantage of the method we propose is that land cover maps at various resolutions are easily available and the method can be adapted to the resolution of available data, or aggregated at the model mesh scale. It would be interesting to have also a higher resolution of the geology map to improve the Kf_s map for smaller catchments. The mapping method could also be improved by introducing spatial variability in each geology * land cover combination, by assigning to each pixel a Kf_s value taken from a lognormal distribution as defined in Table 4. It is far beyond the scope of this paper to investigate which of the two maps in Figure 9 would lead to the best predictions in terms of hydrological modeling, but it would be worth investigating this question further, in order to determine the proper applicability of the proposed mapping methods. Nevertheless, Figure 10 and the results obtained in this study showed that for topsoil horizons, the RB85 pedotransfer function method gives lower Kf_s than Kf_s from the pooled procedure in our study and that additional information such as land cover and geology should be taken into account when mapping topsoil hydraulic properties.

To our knowledge, no study tried to pool data obtained from infiltrometers and different types of positive head infiltration tests. Our study shows that simple relationships can be obtained allowing for pooling initially heterogeneous data sets, and obtaining larger homogeneous data sets for further analysis.

An interesting perspective of this work would be the use of both Kf_s maps in uncalibrated distributed hydrological models (see Vannier et al., 2016) to see if discharge simulation is improved at the regional scale.

CONCLUSIONS

This paper reports on the significant efforts deployed to gather data obtained from infiltration measurements in the Cévennes-Vivarais region. The main challenge of this data set was the diversity of methods used to perform those measurements, which resulted in Kf_s values varying with several orders of magnitude, and the very small number of factors available at all studied sites (geology and land cover only). A method was proposed for pooling all the data sets and deriving an "equivalent" double ring + tension infiltrometer (DR+TI) field-saturated hydraulic conductivity. As geology and land cover were found to be significant discriminating factors on Kf_s

values, they were used to propose a method for mapping topsoil Kf_s in the region. This map was compared to a map based on the RB85 pedotransfer function method. Very different output pattern between the two maps was observed. RB85 values did not fit observed values with our method at each measurement location, highlighting that soil texture alone may not be a good predictor of Kf_s. An interesting perspective of the work is to compare the impact of different Kf_s mapping method on the results of distributed hydrological models.

REFERENCES

Andrieu, J., 2015. Landcover map Ardeche, Ceze and Gardon bassins, ESPRI/IPSL. https://doi.org/10.14768/MISTRALS-HYMEX.1377

Angulo-Jaramillo, R., Vandervaere, J.-P., Roulier, S., Thony, J.-L., Gaudet, J.-P., Vauclin, M., 2000. Field measurement of soil surface hydraulic properties by disc and ring infiltrometers: A review and recent developments. Soil and Tillage Research, 55, 1–2, 1–29.

Ankeny, M.D., Ahmed, M., Kaspar, T.C., Horton, R., 1991. Simple field method for determining unsaturated hydraulic conductivity. Soil Sci. Soc. Am. J., 55, 467–470.

Ayral, P.A., Sauvagnargues-Lesage, S., Gay, S., Bressand, F., 2005. Forecasting flash-floods with an operational model. Aplication in the South-East of France (Gard). In: Begum, S. (Ed.): Flood Risk Management in Europe. Springer, pp. 335–352.

Bagarello, V., Baiamonte, G., Castellini, M., Di Prima, S., Iovino, M., 2014. A comparison between the single ring pressure infiltrometer and simplified falling head techniques. Hydrological Processes, 28, 18, 4843–4853.

Baran, N., Cerdan, O., King C., Saplairoles, M., Thiery, D., 2006. Appui aux actions SCHAPI - BVNE Gardon d'Anduze et Somme, Bassin versant du Touch Rapport « annuel » année 4 janvier 2006 - décembre 2006, BRGM/RP-54996-FR, décembre 2006, 156 pp., http://infoterre.brgm.fr/rapports/RP-54996-FR.pdf

Bonell, M., Purandara, B.K., Venkatesh, B., Krishnaswamy, J., Acharya, H.A.K., Singh, U.V., Jayakumar, R., Chappell, N., 2010. The impact of forest use and reforestation on soil hydraulic conductivity in the Western Ghats of India: Implications for surface and sub-surface hydrology. Journal of Hydrology, 391, 1–2, 47–62.

Bonnet, S., 2012. Cartographie des zones potentielles de production ou d'accumulation du ruissellement de surface en région cévenole. Master 2 « Eau et ressources », Université de Montpellier 2, 98 pp (In French.), available at http://cemadoc.irstea.fr/oa/PUB00035698-cartographie-des-zones-potentielles-production-acc.html

Braud, I., Ayral, P.-A., Bouvier, C., Branger, F., Delrieu, G., Le Coz, J., Nord, G., Vandervaere, J.-P., Anquetin, S., Adamovic, M., Andrieu, J., Batiot, C., Boudevillain, B., Brunet, P., Carreau, J., Confoland, A., Didon Lescot, J.-F., Domergue, J.-M., Douvinet, J., Dramais, G., Freydier, R., Gérard, S., Huza, J., Leblois, E., Le Bourgeois, O., Le Boursicaud, R., Marchand, P., Martin, P., Nottale, L., Patris, N., Renard, B., Seidel, J.-L., Taupin, J.D., Vannier, O., Vincendon, B., Wijbrans, A., 2014. Multi-scale hydrometeorological observation and modelling for flash-flood understanding. Hydrology and Earth System Sciences, 18, 3733–3761.

Braud, I., Vandervaere, J.P., 2015. Analysis of infiltration tests performed in the Claduègne catchment in May-June 2012, contribution to WP3.4 "Documentation and mapping of soil hydraulic properties, soil geometry and vegetation cover of small catchments" of the FloodScale (2012–2015) ANR project, 66 pp. Available at http://mistrals.sedoo.fr/?editDatsId=1321

Cerdan, O., Desprats, JF, King, C., 2004. Appui aux actions SCHAPI au sein de l'arc cévenol. Rapport annuel BRGM/RP-53027-FR, mars 2004, 74 pp. http://infoterre.brgm.fr/rapports/RP-53027-FR.pdf

Clapp, R.B., Hornberger, G.M., 1978. Empirical equations for some soil hydraulic properties. Water Resources Research, 14, 4, 601–604.

Cosby, B.J., Hornberger, G.M., Clapp, R.B., Ginn, T.R., 1984. A statistical exploration of the relationships of soil moisture characteristics to the physical properties of soils. Water Resources Research, 20, 6, 682–690.

Davis, S.H., Vertessy, R.A., Silberstein, R.P., 1999. The sensitivity of a catchment model to soil hydraulic properties obtained by using different measurement techniques. Hydrological Processes, 13, 5, 677–688.

Desprats, J.F., Baran, N., King, C., Ayral, PA, Petelet, E., 2005. Appui aux actions SCHAPI - Gardon d'Anduze, Avène, Touch - Rapport « annuel » 2005 BRGM/RP-53901-FR, Avril, 2005,120 pp ? http://infoterre.brgm.fr/rapports/RP-53901-FR.pdf

Desprats, J.F., Aubert, M., Baghdadi, N., Baran, N., 2007. Appui aux actions SCHAPI - BVNE Gardon d'Anduze et Somme, Bassin versant du Touch, bassin de Nîmes, Rapport annuel « année 5 »- décembre 2007, BRGM/RP-55869-FR, décembre 2007, 170 pp., http://infoterre.brgm.fr/rapports/RP-55869-FR.pdf

Desprats, J.F., Baran, N., Cerdan, O., Fleury, P., Ladouche, B., 2008. Appui aux actions SCHAPI - BVNE Gardon d'Anduze et Somme, Bassin versant du Touch, bassin de Nîmes, Rapport annuel « année 5 »- décembre 2008, BRGM/RP-56745-FR, décembre 2008, 133 pp., http://infoterre.brgm.fr/rapports/RP-56745-FR.pdf

Desprats, J.-F., Cerdan, O, King, C, Marchandise, A., 2010. Cartographie de la perméabilité des sols pour l'aide à la prévision des crues; cas d'étude sur le Gardon d'Anduze. La Houille Blanche, 32–38.

Dunne, T., Black, R.D., 1970. Partial area contributions to storm runo in a small New-England watershed. Water Resources Research, 6, 5,1296–1311.

Ferrer Julià, M., Estrela Monreal, T., Sánchez del Corral Jiménez, A., García Meléndez, E., 2004. Constructing a saturated hydraulic conductivity map of Spain using pedotransfer functions and spatial prediction. Geoderma, 123, 3–4, 257–277.

Garambois, P.A., Roux, H., Larnier, K., Castaings, W., Dartus, D., 2013. Characterization of process-oriented hydrologic model behavior with temporal sensitivity analysis for flash floods in Mediterranean catchments. Hydrology and Earth System Sciences, 17, 2305–2322.

Gaume, E., Bouvier, C., 2004. Analyse hydro-pluviométrique des crues du Gard et du Vidourle des 8 et 9 Septembre 2002. La Houille Blanche, 6, 99–106.

Gonzalez-Sosa, E., Braud, I., Dehotin, J., Lassabatère, L., Angulo-Jaramillo, R., Lagouy, M., Branger, F., Jacqueminet, C., Kermadi, S., Michel, K., 2010. Impact of land use on the hydraulic properties of the topsoil in a small French catchment. Hydrological Processes, 24, 17, 2382–2399.

Horton, R.E., 1933. The role of infiltration in the hydrologic cycle. Transactions – American Geophysical Union, 14, 1, 446–460.

Jarvis, N., 2008. Near-saturated hydraulic properties of macroporous soils. Vadose Zone Journal, 7, 1302–1310.

Jarvis, N., Koestel, J., Messing, I., Moeys, J., Lindahl, A., 2013. Influence of soil, land use and climatic factors on the hydraulic conductivity of soil. Hydrol. Earth Syst. Sci., 17, 12, 5185–5195.

Jorda, H., Bechtold, M., Jarvis, N., Koestel, J., 2015. Using boosted regression trees to explore key factors controlling saturated and near-saturated hydraulic conductivity. European Journal of Soil Science, 66, 4, 744–756.

Laganier, O., Ayral, P.A., Salze, D., Sauvagnargues, S., 2014. A coupling of hydrologic and hydraulic models appropriate for the fast floods of the Gardon River basin (France). Nat. Hazards Earth Syst. Sci., 14, 11, 2899–2920.

Lassabatère, L., Angulo-Jaramillo, R., Soria-Ugalde, J.M., Cuenca, R., Braud, I., Haverkamp, R., 2006. Beerkan estimation of soil transfer parameters through infiltration experiments. Soil Science Society of America Journal, 70, 2, 521–532.

Manus, C., Anquetin, S., Braud, I., Vandervaere, J.P., Viallet, P., Creutin, J.D., Gaume, E., 2009. A modelling approach to assess the hydrological response of small Mediterranean catchments to the variability of soil characteristics in a context of extreme events. Hydrology and Earth System Sciences, 13, 79–87.

Mohanty, B., Kanwar, R.S., Everts, C.J., 1994. Comparison of saturated hydraulic conductivity measurement methods for a Glacial-Till soil. Soil Science Society of America Journal, 58, 3, 672–677.

Naulin, J.P., Payrastre, O., Gaume, E., 2013. Spatially distributed flood forecasting in flash flood prone areas: Application to road network supervision in Southern France. Journal of Hydrology, 486, 88–99.

R Core Team, 2014. R: A language and environment for statistical computing. R Foundation for Statistical Computing, Vienna, Austria. URL http://www.R-project.org/.

Rawls, W.J., Brakensiek, D.L., 1985. Prediction of soil water properties for hydrologic modeling. In: Jones, E.B., Ward, T.J. (Eds.): Watershed Management in the Eighties. ASCE, Denver, pp. 293–299.

Reynolds, W.D., Elrick, D.E., 1991. Determination of hydraulic conductivity using a tension infiltrometer. Soil Sci. Soc. Am. J., 54, 1233–1241.

Ronayne, M.J., Houghton, T.B., Stednick, J.D., 2012. Field characterization of hydraulic conductivity in a heterogeneous alpine glacial till. Journal of Hydrology, 458, 103–109.

Roux, H., Labat, D., Garambois, P.A., Maubourguet, M.M., Chorda, J., Dartus, D., 2011. A physically-based parsimonious hydrological model for flash floods in Mediterranean catchments. Natural Hazards and Earth System Sciences, 11, 9, 2567–2582.

Saulnier, G.M., Le Lay, M., 2009. Sensitivity of flash-flood simulations on the volume, the intensity, and the localization of rainfall in the Cévennes-Vivarais region (France). Water Resources Research, 45, W10425, DOI: 10.1029/2008WR0069056.

Schaap, M.G., Leij, F.J., van Genuchten, M.T., 2001. ROSETTA: a computer program for estimating soil hydraulic parameters with hierarchical pedotransfer functions, J. Hydrol., 251, 163–176.

Vandervaere, J.P., 1995. Caractérisation hydrodynamique du sol in situ par infiltrométrie à disques. Analyse critique des régimes pseudo-permanents, méthodes transitoires et cas des sols encroûtés. Université Joseph Fourier, Grenoble I, Grenoble, France, 9 Octobre 1995, 329 pp, available at https://tel.archives-ouvertes.fr/tel-00694150/

Vandervaere, J.P., Vauclin, M., Elrick, D.E., 2000. Transient flow from tension infiltrometers: II. Four methods to determine sorptivity and conductivity. Soil Science Society of America Journal, 64, 1271–1284.

Vannier, O., Anquetin, S., Braud, I., 2016. Investigating the role of geology in the hydrological response of Mediterranean catchments prone to flash-floods: regional modelling study and process understanding. Journal of Hydrology, 541 Part A, 158–172.

Verbist, K.M.J., Cornelis, W.M., Torfs, S., Gabriels, D., 2013. Comparing methods to determine hydraulic conductivities on stony soils. Soil Science Society of America Journal, 77, 1, 25–42.

Vereecken, H., Weynants, M., Javaux, M., Pachepsky, Y., Schapp, M.G., van Genuctchen, M.T., 2010. Using pedotransfer functions to estimate the van Genuchten-Mualem soil hydraulic conductivity properties: a review. Vadose Zone Journal, 9, 795–820.

Vincendon, B., Édouard, S., Dewaele, H., Ducrocq, V., Lespinas, F., Delrieu, G., Anquetin, S., 2016. Modeling flash floods in southern France for road management purposes. Journal of Hydrology, 541 Part A, 190–205.

Xu, X., Lewis, C., Liu, W., Albertson, J.D., Kiely, G., 2012. Analysis of single-ring infiltrometer data for soil hydraulic properties estimation: Comparison of BEST and Wu methods. Agricultural Water Management, 107, 34–41.

Wösten, J.H.M., Pachepsky, Y.A., Rawls, W.J., 1999. Development and use of a database of hydraulic properties of European soils. Geoderma, 90, 169–185.